Liquid-solid transition of the ferromagnetic Heisenberg fluid: Simulation, density functional, and perturbation theories

E. Lomba
Instituto de Quimica Fisica Rocasolano, Consejo Superior de Investigaciones Científicas, Serrano 119, E-28006 Madrid, Spain

J. J. Weis
Laboratoire de Physique Théorique et Hautes Energies, Université de Paris XI, Bâtiment 211, F-91405 Orsay Cedex, France

C. F. Tejero
Facultad de Ciencias Físicas, Universidad Complutense de Madrid, E-28040 Madrid, Spain

(Received 9 March 1998)

The fluid-solid equilibrium of a system of hard spheres with embedded classical Heisenberg spins is studied by means of computer simulation and various combinations of density functional theories with the spin-spin contributions treated at the level of first-order perturbation theory. The phase boundaries are determined from the simulation data using free energy calculations in the ferromagnetic and isotropic phases. Estimates of the location of the Curie line in the solid are extracted from inspection of the evolution of magnetization with temperature. The agreement between theory and simulation is relatively good for the ferromagnetic transition and merely qualitative as far as the fluid-solid transition is concerned. The theoretical approach investigated here tends to underestimate the stability of the liquid phase. [S1063-651X(98)13609-7]

PACS number(s): 61.20.Gy, 64.60.Cn, 71.10.−w

I. INTRODUCTION

The classical Heisenberg model is among the simplest ones to study systems of particles with continuously varying internal degrees of freedom. The model has been extensively used in lattice simulations, especially to determine the critical exponents associated with the paramagnetic-ferromagnetic phase transition [1,2]. However, the continuum version of the model, in which the spins are not confined to lattice positions and the interaction between pairs of spins is represented by a continuous function of their distance, is of interest too, presenting an even richer phase diagram comprising both magnetic and nonmagnetic gases, liquids, and solids.

The topologically different diagrams of the continuum Heisenberg model, depending on the ratio of the integrated strength of the exchange interaction to the spin-independent interaction, have been established by Hemmer and Imbro [3] within mean field (MF) theory and more recently by Tavares and co-workers [4,5] using both MF and a more refined modified mean field (MMF) density functional theory (DFT). More quantitative results have been obtained from Monte Carlo (MC) [6–9] simulations for the case where the spin-independent interaction between pairs of particles is of the hard-sphere type. Thus the Curie line for the order-disorder transition has been located accurately by means of a finite size scaling analysis [8] and the liquid-vapor coexistence curve determined from Gibbs ensemble MC (GEMC) calculations [7,5]. Although the existing simulation results suggest that the Curie line terminates at a critical end point on the vapor side of the coexistence curve, implying the existence of a magnetic critical point, precise locations of the parameters of the critical end point and magnetic critical point are still lacking, mainly because of the absence of an estimate of finite size effects on the coexistence curve.

In this paper we focus primarily on the liquid-solid coexistence. Assuming a face-centered-cubic (fcc) structure of the solid near melting we first determine the Curie line separating the paramagnetic from the ferromagnetic solid. Below the Curie temperature, liquid-solid coexistence will occur between a ferromagnetic liquid and a ferromagnetic solid. The coexistence densities can be obtained from knowledge of the absolute free energies of the two phases. The liquid and solid free energies are determined in a Monte Carlo simulation by means of a reversible path linking a state of the system to that of a system in an infinitely strong external field that completely aligns the spins. The free energy of the latter state, in turn, is evaluated by straightforward thermodynamic integration.

The knowledge of exact absolute free energies in the liquid and solid phases further enable us to test in a quantitative way recent density functional theories [10–13]. Some of these intended to establish the phase diagram of dipolar fluids, which bears a close resemblance to the present one. Although the dipolar system may be a more realistic model for ferrofluids, its study, by theory [10,14] or simulation [6], is vastly more complicated than the Heisenberg system, due to the long range of the dipolar interaction and the concomitant dependence of properties on sample shape and boundaries. In view of these difficulties, not encountered in the present model where the interactions are strictly short ranged, no ''exact'' free energies have been reported yet for the dipolar ferromagnetic phases allowing a test of the theories.

In the following section we briefly summarize the model. Section III is devoted to a brief presentation of the key elements of the various DFT perturbation approaches explored in this work. A detailed description of the simulation techniques used to attain a complete description of the fluid-solid transition between ferromagnetic phases can be found in Sec.

IV. Finally, the most significant results are presented and commented upon in Sec. V.

II. MODEL

In accordance with previous simulations of the gas-liquid coexistence curve [5,7] and the Curie line [8], the interaction between two particles $u(r,\omega_1,\omega_2)$ is taken to be the sum of a hard core part

$$u_0(r)=\begin{cases}+\infty, & r\leqslant\sigma\\ 0, & r>\sigma\end{cases} \tag{1}$$

and a spin part

$$u_{ss}(r,\omega_1,\omega_2)=J(r)\mathbf{s}_1\cdot\mathbf{s}_2. \tag{2}$$

$$J(r)=-J\frac{e^{-z(r/\sigma-1)}}{r/\sigma}\quad(\sigma<r<r_c=\delta\sigma), \tag{3}$$

where $\mathbf{s}_i$ is a unit vector in the direction of the dipole moment, $r=|\mathbf{r}_1-\mathbf{r}_2|$, and σ is the hard sphere diameter. In order to be consistent with previous works [5,8], the cutoff distance of the Yukawa potential was set to $\delta=2.5$ and $z=1$. A thermodynamic state of the system will be conveniently characterized by the reduced density $\rho^*=\rho\sigma^3$ (or the packing fraction $\eta=\pi\rho^*/6$) and the reduced temperature $T^*=1/J^*=k_BT/J$. The coupling constant J is taken to be positive, thereby favoring parallel configurations (ferromagnetic).

III. DENSITY FUNCTIONAL AND PERTURBATION THEORY

The presence of a hard-core interaction suggests the construction of an approximate Helmholtz free energy of the Heisenberg model $F[\rho]$, the square brackets denoting a functional dependence, by means of first-order perturbation theory around a hard-sphere reference system [15,16]. Accordingly, we write

$$F[\rho]\simeq F_0[\rho]+F_1[\rho], \tag{4}$$

where $F_0[\rho]$ is the free energy of the hard-sphere reference system and $F_1[\rho]$ the first-order perturbation term. The right-hand side of Eq. (4) is known to be an upper bound of $F[\rho]$ irrespective of the choice of the reference system. This exact result will be used to estimate $F[\rho]$ by minimizing the upper bound with respect to a free parameter of the reference system.

The reference system Helmholtz free energy $F_0[\rho]$ can be split as a sum of the ideal and excess contributions, i.e.,

$$F_0[\rho]=F_0^{\mathrm{id}}[\rho]+F_0^{\mathrm{ex}}[\rho], \tag{5}$$

where

$$\beta F_0^{\mathrm{id}}[\rho]=\int d\mathbf{r}\ \rho(\mathbf{r})\{\ln[\rho(\mathbf{r})\Lambda^3)-1]\}+N\int d\omega\ \alpha(\omega)\ln[4\pi\alpha(\omega)], \tag{6}$$

with $\beta=1/k_BT$ the inverse temperature, N the number of particles, and Λ the thermal de Broglie wavelength. In writing Eq. (6) it has been assumed that the one-particle density $\rho(\mathbf{r},\omega)$ factorizes into translational and spin variables

$$\rho(\mathbf{r},\omega)=\rho(\mathbf{r})\alpha(\omega), \tag{7}$$

with normalizations

$$\int d\omega\ \alpha(\omega)=1 \tag{8}$$

and

$$\int d\mathbf{r}\ \rho(\mathbf{r})=N. \tag{9}$$

While a variety of approximation schemes have been proposed for the excess free energy [16] (see below), the perturbation term associated with the attractive part of the interaction (2) has so far mostly been evaluated in a MF [4,13,17] or MMF [4,18,19] approximation. In the MF approximation, the free energy is given by

$$\beta F_1^{\mathrm{MF}}[\rho]=\frac{1}{2}\int d\omega_1\int d\omega_2(\mathbf{s}_1\cdot\mathbf{s}_2)\alpha(\omega_1)\alpha(\omega_2)\times\int d\mathbf{r}\ \rho(\mathbf{r})\int d\mathbf{r}'\rho(\mathbf{r}')\beta J(|\mathbf{r}-\mathbf{r}'|) \tag{10}$$

and in the MMF approximation reads

$$\beta F_1^{\mathrm{MMF}}[\rho]=\frac{1}{2}\int d\omega_1\int d\omega_2\alpha(\omega_1)\alpha(\omega_2)\times\int d\mathbf{r}\ \rho(\mathbf{r})\int d\mathbf{r}'\rho(\mathbf{r}')[1-e^{-\beta J(|\mathbf{r}-\mathbf{r}'|)\mathbf{s}_1\cdot\mathbf{s}_2}]. \tag{11}$$

The basic simplification in MMF theory is to approximate the two-particle correlation function by its low-density limit and in MF theory by its large-distance limit. Note that MF theory gives a nonvanishing result only in the ferromagnetic phase. In the following subsections we will specify the different free energy contributions for the fluid and solid phases. Once an approximate free energy functional is chosen, the equilibrium density distribution is obtained by minimization of the free energy functional and the coexistence densities by requiring that the pressures and chemical potentials of the liquid and solid phases be equal.

A. Ferromagnetic liquid

For the fluid phase the one-particle density is

$$\rho(\mathbf{r},\omega)=\rho\alpha(\omega), \tag{12}$$

where ρ is the (uniform) density of the fluid. In this case the ideal free energy per particle yields

$$\beta f_0^{\mathrm{id}}[\rho]=\ln(\rho\Lambda^3)-1+\int d\omega\ \alpha(\omega)\ln[4\pi\alpha(\omega)], \tag{13}$$

while the excess free energy per particle will be determined from the Carnahan-Starling [20] equation of state to give

$$\beta f_0^{\mathrm{ex}}[\rho]=\frac{\eta(4-3\eta)}{(1-\eta)^2}. \tag{14}$$

The perturbation term per particle in the MF approximation is

$$\beta f_1^{\mathrm{MF}}[\rho]=\frac{1}{2}\rho\int d\omega_1\int d\omega_2(\mathbf{s}_1\cdot\mathbf{s}_2)\alpha(\omega_1)\alpha(\omega_2) \times\int d\mathbf{r}\ \beta J(r). \tag{15}$$

One can note that if the system is magnetized in the direction **n** (**n** being the unit vector along the preferred direction of alignment of the spins) then the integral over orientations in Eq. (15) is

$$\left(2\pi\int_{-1}^{1}du\ u\alpha(u)\right)^2, \tag{16}$$

where $u=\mathbf{s}\cdot\mathbf{n}=\cos\theta$. In the MMF approximation

$$\beta f_1^{\mathrm{MMF}}[\rho]=\frac{1}{2}\rho\int d\omega_1\int d\omega_2\alpha(\omega_1)\alpha(\omega_2) \times\int d\mathbf{r}[1-e^{-\beta J(r)\mathbf{s}_1\cdot\mathbf{s}_2}]. \tag{17}$$

To proceed further a parametrization of $\alpha(\omega)$ is needed. One possibility is to expand $\alpha(\omega)$ in terms of Legendre polynomials

$$\alpha(\omega)=\frac{1}{2\pi}\sum_{l=0}^{\infty}\alpha_l P_l(\cos\theta) \tag{18}$$

as was done by Tavares *et al.* in Ref. [4]. Once the free energy is constructed using Eqs. (13), (14), and (17), one simply proceeds as usual in DFT, searching for the minimum of the functional, in this case sampling the parameter space defined by the orientational order coefficients α_l. This procedure, though perfectly feasible in the present instance, might be a somewhat delicate numerical task in certain cases [11].

An alternative parametrization is to adopt a simple functional form for $\alpha(\omega)$, e.g.,

$$\alpha(\omega)=Ae^{BP_1(\cos\theta)}, \tag{19}$$

which is well known in the study of orientational transitions in liquid crystals [21,22] and is a straightforward result in simple mean field approaches [13]. Here B plays the role of an *effective field* acting on each spin induced by the magnetic ordering in the medium. With this single order-parameter approximation, the normalization of $\alpha(\omega)$ yields

$$A=\frac{1}{4\pi}\frac{B}{\sinh B}, \tag{20}$$

leading to a spin contribution of the ideal free energy given by

$$\int d\omega\ \alpha(\omega)\ln[4\pi\alpha(\omega)]=B\coth B-1-\ln\left(\frac{\sinh B}{B}\right). \tag{21}$$

The perturbation free energy can also be integrated explicitly in the MF approximation leading to

$$\beta f_1^{\mathrm{MF}}[\rho]=-\frac{24\eta\lambda}{T^*}\left[\coth B-\frac{1}{B}\right]^2, \tag{22}$$

where

$$\lambda=\frac{1}{2}\left[\left(\frac{1}{z}+\frac{1}{z^2}\right)-e^{-z(\delta-1)}\left(\frac{\delta}{z}+\frac{1}{z^2}\right)\right], \tag{23}$$

i.e., $\lambda=0.6095$ for the cutoff distance considered in the simulations.

For the MMF approximation, if one uses Neumann's expansion of the exponential in Eqs. (17) and (18), the orthogonality properties of the Legendre polynomials tell us that the free energy can be expressed as

$$\beta f_1^{\mathrm{MMF}}[\rho]=-\frac{1}{2}\sum_{l=0}^{\infty}(2l+1)^2\left(\frac{i_l(B)}{i_0(B)}\right)^2 u_l(\eta,T^*), \tag{24}$$

i.e., a series expansion that depends on a single parameter B, where

$$i_l(x)=\sqrt{\frac{\pi}{2x}}I_{l+1/2}(x), \tag{25}$$

with $I_{l+1/2}(x)$ the modified spherical Bessel functions of the first kind [23], and

$$u_l(\eta,T^*)=24\eta\int_1^{\delta}dx\ x^2\left(\frac{i_l[\beta J(x)]}{2l+1}-\delta_{l0}\right), \tag{26}$$

with

$$\beta J(x)=\frac{1}{xT^*}e^{-z(x-1)}. \tag{27}$$

This expression is identical to Eq. (16) in Ref. [5] with the orientational order parameters α_l defined in terms of a single effective field B,

$$\alpha_l=\frac{2l+1}{2}\frac{i_l(B)}{i_0(B)}. \tag{28}$$

It turns out that for the ferromagnetic systems we are here dealing with, the multiple-parameter minimization implicit in Eq. (18) when all α_l are considered free and the single-

parameter minimization lead to identical results. Consequently, we will here retain the simpler one-parameter form in our calculations.

Note that the minimization with respect to the order parameter B can be explicitly done in the MF approximation, leading to

$$\frac{B_m^2}{B_m \coth B_m - 1} = \frac{48\eta\lambda}{T^*}, \tag{29}$$

where B_m is the order parameter at the minimum. When $B_m \to 0$, $B_m^2/(B_m \coth B_m - 1) \to 3$, yielding the Curie line of the fluid phase

$$T_c^* = 16\lambda\,\eta. \tag{30}$$

Using similar arguments, the Curie line of the fluid phase in the MMF approximation can be shown to be given by

$$u_1(\eta, T_c^*) = \frac{1}{3}, \tag{31}$$

a result also arrived at in Refs. [10] and [4].

B. Ferromagnetic solid

In the solid phase the local density is given by

$$\rho(\mathbf{r},\omega) = \rho(\mathbf{r})\alpha(\omega), \tag{32}$$

where $\rho(\mathbf{r})$ describes the periodic distribution of particles centered around the lattice sites of the Bravais crystal. In the hard-sphere solid $\rho(\mathbf{r})$ can be accurately parametrized as a sum of identical normalized Gaussians [24,25], i.e.,

$$\rho(\mathbf{r}) = \left(\frac{\gamma}{\pi}\right)^{3/2} \sum_{i=1}^{N} e^{-\gamma(\mathbf{r}-\mathbf{R}_i)^2}, \tag{33}$$

where γ measures the inverse width of the Gaussians and the sum runs over the Bravais lattice vectors $\{\mathbf{R}_i\}$. Since in a solid the Gaussians are very narrow, the translational contribution to Eq. (6) can be approximated by its asymptotic large-γ form leading to the ideal free energy per particle

$$\beta f_0^{\mathrm{id}}[\rho] = 3\ln\left(\frac{\Lambda}{\sigma}\right) + \frac{3}{2}\ln\left(\frac{\gamma\sigma^2}{\pi}\right) - \frac{5}{2} + \int d\omega\ \alpha(\omega)\ln[4\pi\alpha(\omega)]. \tag{34}$$

The excess free energy of the hard-sphere solid has been considered in two slightly different approaches, the generalized effective liquid approximation (GELA) [26,27] and the modified weighted density approximation (MWDA) [28–30], which has recently been applied by Groh and Dietrich [11] to describe the fluid-solid transition in dipolar fluids. In the first instance, we have adopted a perturbative approach, i.e., the hard-sphere solid, approximated in the GELA, is considered to be a pure reference system, with a lattice parameter known in advance, and then the perturbation term to the free energy is minimized following the Gibbs-Bogoliubov variational principle. We will first focus on the GELA since our treatment leads in this case to much simpler quasianalytical results.

TABLE I. Inverse width of the Gaussian $\gamma^* = \gamma_m\sigma^2$ and effective liquid density $\hat{\eta}_m$ of the hard-sphere fcc solid as obtained from the GELA.

η	γ^*	$\hat{\eta}_m$
0.50	56.4	0.331
0.51	68.0	0.323
0.52	80.9	0.317
0.53	95.6	0.313
0.54	112.7	0.309
0.55	132.8	0.305
0.56	156.6	0.302
0.57	185.1	0.300
0.58	219.9	0.297
0.59	262.4	0.295
0.60	315.3	0.293
0.61	381.8	0.291
0.62	467.3	0.290
0.63	578.6	0.288
0.64	727.8	0.286

In the GELA the excess free energy per particle of the solid $\beta f_0^{\mathrm{ex}}[\rho]$ is mapped onto that of an effective uniform fluid [26,27], i.e.,

$$\beta f_0^{\mathrm{ex}}[\rho] = \frac{\hat{\eta}(4-3\hat{\eta})}{(1-\hat{\eta})^2}, \tag{35}$$

where $\hat{\eta} = \hat{\eta}(\eta,\gamma)$ denotes the effective packing fraction that is used to represent the solid (η being the average packing fraction of the solid) and we have assumed that the hard-sphere fluid can be described by the Carnahan-Starling equation of state (see [26,27] for details).

By minimizing the variational free energy $\beta f_0^{\mathrm{id}}[\rho] + \beta f_0^{\mathrm{ex}}[\rho]$ with respect to γ, for a given average solid density and a crystal structure (here the fcc hard-sphere solid), the free energy of the reference solid reads

$$\beta f_0[\rho] = f_{\mathrm{HS}}(\eta) + \int d\omega\ \alpha(\omega)\ln[4\pi\alpha(\omega)], \tag{36}$$

where

$$f_{\mathrm{HS}}(\eta) = 3\ln\left(\frac{\Lambda}{\sigma}\right) + \frac{3}{2}\ln\left(\frac{\gamma_m\sigma^2}{\pi}\right) - \frac{5}{2} + \frac{\hat{\eta}_m(4-3\hat{\eta}_m)}{(1-\hat{\eta}_m)^2}, \tag{37}$$

where $\gamma_m = \gamma_m(\eta)$ is the value of the order parameter at the minimum and $\hat{\eta}_m = \hat{\eta}(\eta, \gamma_m(\eta))$. Note that since the hard-core part (1) has no spin-spin interaction, the angular dependence $\alpha(\omega)$ does not contribute to the excess part of the free energy, the resulting free energy of the reference solid being the same as that of the hard-sphere solid (without spin) plus an ideal contribution coming from the angular distribution of the spin variables. Since this contribution is the same for the

fluid and solid phases, the change of stability between the fluid and solid reference systems is found at $\eta=0.517$ [27]. In Table I we have gathered the values of $\gamma^*=\gamma_m\sigma^2$ and $\hat{\eta}_m$ of the fcc hard-sphere solid for different average solid densities.

Using the parametrized form (19) for $\alpha(\omega)$ and performing the angular integrations in the translational part of Eq. (10), the perturbation term per particle in the MF approach reads

$$\beta f_1^{\mathrm{MF}}[\rho]=-\frac{1}{4T^*}R(\eta)\left[\coth B-\frac{1}{B}\right]^2, \tag{38}$$

where

$$R(\eta)=e^{z^2/2\gamma^*}\sum_j \frac{z}{x_j}e^{z(-x_j+1)}\left[\mathrm{erf}\left(\frac{z+\gamma^*(\delta-x_j)}{\sqrt{2\gamma^*}}\right)-\mathrm{erf}\left(\frac{z+\gamma^*(1-x_j)}{\sqrt{2\gamma^*}}\right)\right]-e^{z^2/2\gamma^*}\sum_j \frac{z}{x_j}e^{z(x_j+1)}\times\left[\mathrm{erf}\left(\frac{z+\gamma^*(\delta+x_j)}{\sqrt{2\gamma^*}}\right)-\mathrm{erf}\left(\frac{z+\gamma^*(1+x_j)}{\sqrt{2\gamma^*}}\right)\right], \tag{39}$$

where $x_j(\eta)=|\mathbf{R}_j|/\sigma$ and $\mathrm{erf}(x)$ is the error function. For the MMF approximation we use again Neumann's expansion of the exponential in Eqs. (17) and (18), together with the orthogonality properties of the Legendre polynomials, to get

$$\beta f_1^{\mathrm{MMF}}[\rho]=-\frac{1}{2}\sum_{l=0}^{\infty}(2l+1)^2\left(\frac{i_l(B)}{i_0(B)}\right)^2 v_l(\eta,T^*), \tag{40}$$

with

$$v_l(\eta,T^*)=\left(\frac{\gamma^*}{2\pi}\right)^{1/2}\sum_j \frac{1}{x_j}\int_1^{\delta}dx\ x^2\left(\frac{i_l(\beta J(x))}{2l+1}-\delta_{l0}\right)\times[e^{-\gamma^*(x-x_j)^2/2}-e^{-\gamma^*(x+x_j)^2/2}]. \tag{41}$$

Again, the minimization with respect to the order parameter can be exactly computed in the MF approximation to find

$$\frac{B_m^2}{B_m\coth B_m-1}=\frac{1}{2T^*}R(\eta), \tag{42}$$

yielding for the Curie line of the solid phase

$$T_c^*=\frac{1}{6}R(\eta), \tag{43}$$

which reduces to the evaluation of a lattice sum for each average solid density. Using similar arguments, the Curie line of the solid phase in the MMF approximation can be shown to be given by

$$v_1(\eta,T_c^*)=\frac{1}{3}. \tag{44}$$

These perturbative contributions remain identical in the MWDA treatment, in which again the solid is mapped onto a uniform system at a weighted density (see [28] and [11] for more details). In contrast to our treatment in the GELA, when using the MWDA, we have followed Groh and Dietrich, who, from a DFT perspective, minimize the full free energy functional built from the ideal, reference, and perturbation contributions. This implies that the lattice parameter and the effective field B are variables that enter the minimization process. Again, one could also use as minimization parameters all the α_l from Eq. (28), but at least in our case this leads to identical results, as it happens with the ferromagnetic liquid. It can be noted that the MF theory described above is similar to the van der Waals–type theory proposed by Oukouiss and Baus [13], except for the fact that in the latter theory the hard-sphere free energy is treated in the (numerically poor) free volume approximation.

IV. SIMULATIONS

The free energies of the liquid and solid phases were calculated by means of thermodynamic integration. In this method the absolute free energy of a state is related to the (known) free energy of a reference state via a reversible path linking both states. For the ferromagnetic phases under investigation the reference state that asserts itself is a state where the spins are perfectly aligned. The actual state is transformed to the perfectly aligned one by coupling the spins to an external aligning field. Such a procedure was applied previously by Veerman and Frenkel [31] to determine the free energy of the smectic phase of spherocylinders.

The Hamiltonian of the spin system in a constant field of magnitude λ is

$$H_\lambda=H_0-\lambda\sum_i \cos\ \theta_i, \tag{45}$$

where H_0 is the Hamiltonian of the system in the absence of the field and θ_i is the angle of spin i with the field. The change in free energy entailed by the field is given by

$$F_\lambda=F_0-\int_0^{\lambda}d\lambda'\left\langle\sum_i \cos\ \theta_i\right\rangle_{\lambda'}, \tag{46}$$

where $\langle\ \rangle_{\lambda'}$ denotes averaging over the system with the Hamiltonian $H_{\lambda'}$.

Let us further consider an ideal (noninteracting) system of spins in an external field. A relation similar to Eq. (46) holds,

$$F_\lambda^{\mathrm{id}}=F_0^{\mathrm{id}}-\int_0^{\lambda}d\lambda'\left\langle\sum_i \cos\ \theta_i\right\rangle_{\lambda'}^{\mathrm{id}}, \tag{47}$$

where $\langle\ \rangle_{\lambda'}^{\mathrm{id}}$ denotes averaging over the system with the Hamiltonian

$$H_{\lambda'}^{\mathrm{id}}=-\lambda\sum_i \cos\ \theta_i. \tag{48}$$

If one now remarks [31] that in the limit of an infinitely strong field ($\lambda\to\infty$,) $F_\lambda-F_\lambda^{\mathrm{id}}\to F_p$, the free energy of the parallel (perfectly aligned) system, then

TABLE II. Contributions to the free energy of the spin system in fluid and solid reference states as obtained from the MC simulation. Δ denotes the last term on the right-hand side of Eq. (51).

ρ^*	T^*	$\beta F_{\rm HS}/N$	$\beta F_p/N$	$\beta F^{\rm id}_{\lambda_0}/N$	$\beta/N\int_0^{\lambda_0} d\lambda\langle\Sigma_i \cos\theta_i\rangle_{\lambda'}$	$\beta\Delta/N$	$\beta F/N$
0.92	1	3.498 [a]	−5.162	−94.702	98.033	0.156	−1.675
0.92	3	3.498 [a]	+0.613	−94.702	97.010	0.057	+2.978
1.10	1	5.653 [b]	−5.025	−94.702	98.220	0.187	−1.324
1.10	3	5.653 [b]	+2.097	−94.702	97.203	0.067	+4.665

[a]From the Carnahan-Starling equation of state [20].
[b]From the Hall equation of state [35].

$$F_0 = F_p + F_0^{\rm id} + \int_0^{\infty} d\lambda' \left[\left\langle \sum_i \cos\theta_i \right\rangle_{\lambda'} - \left\langle \sum_i \cos\theta_i \right\rangle_{\lambda'}^{\rm id} \right] \tag{49}$$

$$\simeq F_p + F_0^{\rm id} + \int_0^{\lambda_m} d\lambda' \times \left[\left\langle \sum_i \cos\theta_i \right\rangle_{\lambda'} - \left\langle \sum_i \cos\theta_i \right\rangle_{\lambda'}^{\rm id} \right]. \tag{50}$$

The last relation follows from the fact that for sufficiently large λ_m the contribution of the neglected term (integral from λ_m to ∞) will be vanishingly small.

Finally, from a numerical point of view, it will be convenient to split the integral in Eq. (49) into two parts

$$F_0 = F_p + F_0^{\rm id} + \int_0^{\lambda_0} d\lambda' \left\langle \sum_i \cos\theta_i \right\rangle_{\lambda'} + \int_{\lambda_0}^{\lambda_m} d\lambda' \left[\left\langle \sum_i \cos\theta_i \right\rangle_{\lambda'} - \left\langle \sum_i \cos\theta_i \right\rangle_{\lambda'}^{\rm id} \right], \tag{51}$$

where

$$F^{\rm id}_{\lambda_0} = -\frac{N}{\beta} \ln\left[\frac{\sinh \beta\lambda_0}{\beta\lambda_0} \right] \tag{52}$$

is defined so that it vanishes in the zero field limit. This is consistent with the definition of the ideal free energy in Eq. (6), where the contribution from the rotational degrees of freedom vanishes in the uniform system limit $[\alpha(\omega) = 1/4\pi]$.

For $\lambda < \lambda_0$ the contribution from the ideal term has been evaluated analytically. For $\lambda > \lambda_0$ it is preferable not to separate the two terms; as remarked in Ref. [31], if both terms in the integrand were calculated separately, the difference between the two terms would become smaller than the statistical error on either term.

Following the strategy suggested by Veerman and Frenkel [31], each trial θ_i is then sampled from the probability distribution

$$P(\theta) \propto \exp(\beta\lambda \cos\theta). \tag{53}$$

If no overlap occurs, the trial move is accepted and

$$\cos\theta_i|_{\lambda} - \cos\theta_i|_{\lambda,{\rm id}} = 0. \tag{54}$$

If no overlap occurs the trial move is rejected and

TABLE III. Thermodynamic properties of the Heisenberg system at the densities $\rho^* = 0.92$ (liquid) and $\rho^* = 1.1$ (solid). m is the magnetization of the system.

		$\rho^* = 0.92$			$\rho^* = 1.10$
Theory	$\beta F/N$	m	Theory	$\beta F/N$	m
		$T^* = 1$			
RZH	−1.672	0.933			
			MWDA	−4.066	0.970
MMF	−1.530	0.946			
			GELA	−3.450	0.968
MF	−0.248	0.923	GELA	−0.780	0.948
MC	−1.68(2)	0.935(1)		−1.32(3)	0.949
		$T^* = 3$			
RZH	2.960	0.759			
			MWDA	4.345	0.838
MMF	3.177	0.714			
			GELA	4.629	0.836
MF	3.246	0.698	GELA	4.79	0.821
MC	2.98(2)	0.764(2)		4.67(3)	0.82

$$\cos\,\theta_i|_\lambda - \cos\,\theta_i|_{\lambda,\mathrm{id}} = \cos\,\theta_i^{\mathrm{old}}|_\lambda - \cos\,\theta_i^{\mathrm{new}}|_{\lambda,\mathrm{id}}. \quad (55)$$

At this point we are still left with the calculation of the free energy of the parallel system. This is simply the system where particles interact by a Yukawa potential (in addition to the hard-sphere interaction) and the free energy is easily obtained by perturbation around the hard-sphere value, i.e.,

$$F_p = F_{\mathrm{HS}} + \int_0^1 d\lambda \left\langle \frac{1}{2}\sum_{i\neq j} J(r_{ij}) \right\rangle_\lambda , \quad (56)$$

where the average is taken over a system with an interparticle potential

$$u_\lambda(r) = u_0(r) + \lambda J(r). \quad (57)$$

V. RESULTS

A. Simulations

The first goal of our investigation was to locate the paramagnetic solid–ferromagnetic solid transition. This was done by recording, at a fixed density, the magnetization of a 512-particle fcc crystal as a function of temperature and estimating the critical temperature from the inflection point of the curve. Such an estimate, ignoring finite size effects, can be expected to be only qualitative. However, a comparison, in Ref. [8], with the more precise value of the transition temperature obtained from the intersection point of the fourth-order Binder cumulant [32] for the magnetization plotted as a function of temperature for different system sizes showed that this estimate is in fact quite accurate. Therefore, we did not apply this more time consuming procedure here. The critical temperatures are approximately $T^*=6.7$ and $T^*=7.3$ for the densities $\rho^*=1.1$ and 1.2, respectively.

The free energy $\beta F/N$ was calculated along the lines detailed in Sec. IV, using the canonical MC method, at the densities $\rho^*=0.92$ (liquid) and $\rho^*=1.10$ (solid) and the two temperatures $T^*=1$ and 3. The number of spins was 512. The different contributions to $\beta F/N$ are summarized in Table II. The free energy of the parallel system $\beta F_p/N$ [cf. Eq. (56)] was evaluated using a five point Gauss-Legendre (GL) quadrature. In fact, the integrand varies very little with λ (the difference of the averages appearing in the integrand for $\lambda=0$ and 1 being only 0.02) so that a first-order perturbation would be a good approximation [33]. The integrals in Eq. (51) were evaluated using a six-point GL quadrature and the values $\beta\lambda_0=100$ and $\beta\lambda_m=50\,000$. For each value of λ averages were taken over runs involving between 30 000 and 40 000 trial moves per particle (after equilibration). The free energy along an isotherm was obtained by integration of the pressure

$$\frac{p}{kT} = \rho + \left(\frac{p}{kT}\right)_{\mathrm{HC}} + \left(\frac{p}{kT}\right)_{\mathrm{spin}}, \quad (58)$$

which is the sum of the hard-core part $(p/kT)_{\mathrm{HC}}$ and the spin part $(p/kT)_{\mathrm{spin}}$ given by

$$\left(\frac{p}{kT}\right)_{\mathrm{spin}} = -\frac{4\pi\rho^2}{18kT}\int dr\; r^3 J'(r) h_\Delta(r). \quad (59)$$

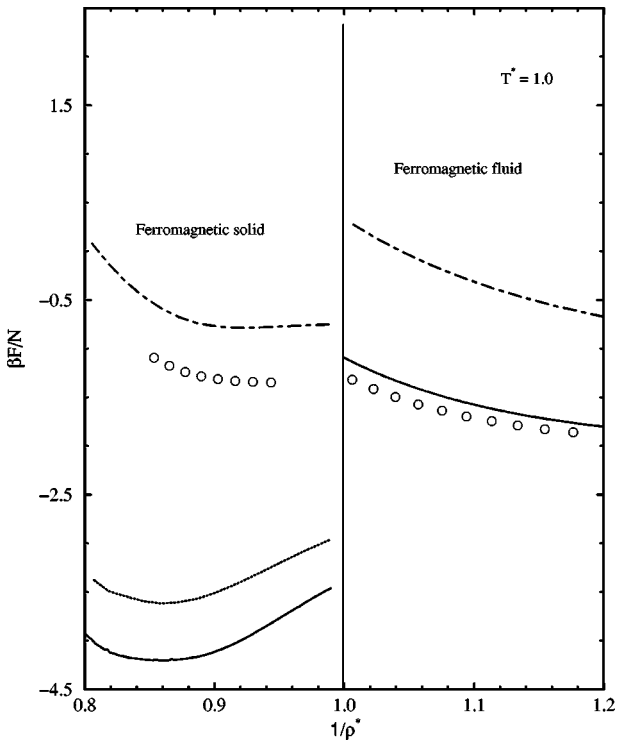

FIG. 1. Free energy at $T^*=1$. Simulation data are represented by circles. A dash-dotted line denotes MF results, which include the GELA in the solid, and a dotted line stands for the GELA plus the MMF data. A solid line represents MMF data in the liquid phase and the MWDA plus the MMF data in the solid.

In Eq. (59) $J'(r)$ is the derivative of $J(r)$ and $h_\Delta(r)$ the projection of the pair distribution function on $\mathbf{s}_1\cdot\mathbf{s}_2$. We note that, owing to the discontinuity of the potential at $r=r_c$, a δ-function contribution arises that is quite significant in the ferromagnetic phase. It is given by

$$\left(\frac{p}{kT}\right)_c = -\frac{4\pi\rho^2}{18kT} r_c^3 J'(r_c) h_\Delta(r_c). \quad (60)$$

Along the isotherm $T^*=1$, the pressure was calculated in the density intervals $\rho^*=0.85-1.00$ (liquid) and $\rho^*=1.06-1.16$ (solid) and along the isotherm $T^*=3$ in the intervals $\rho^*=0.90-1.00$ (liquid) and $\rho^*=1.02-1.14$ (solid); the results were fitted to simple polynomial expressions.

For comparison we include the free energy values obtained in the ferromagnetic liquid phase using an integral equation technique recently devised to deal with inhomogeneous systems [34]. The reference Zerah-Hansen (RZH) closure relation used is especially designed to reproduce the zero field singularities of the magnetic susceptibility and although free energies are only accessible through thermodynamic integration, the results obtained are in absolute accordance with the simulation data, as can be appreciated in Table II. Coexistence densities, summarized in Table III, were obtained from the equality of the pressures and chemical potentials $\beta\mu=\beta F/N+\beta p$ in the two phases.

B. Density functional theory

The key quantity in a thermodynamic description is doubtless the free energy. It is then worthwhile assessing the

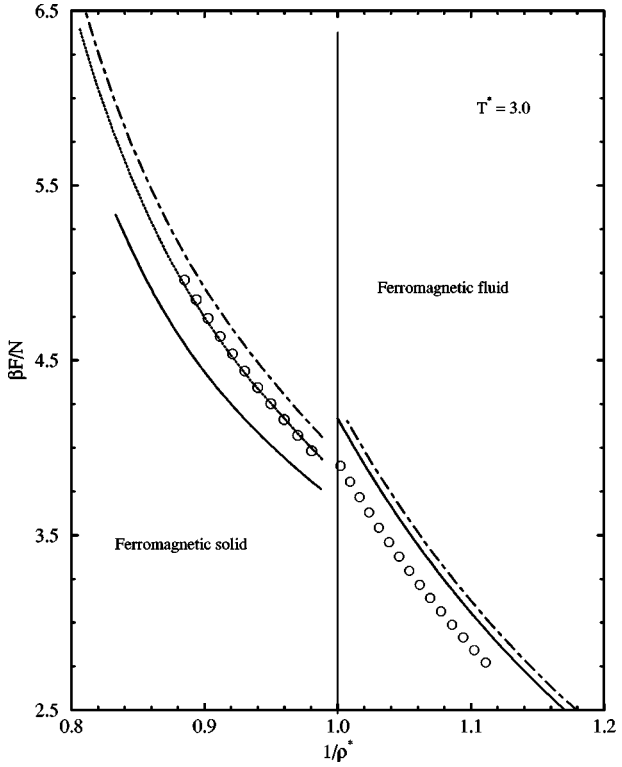

FIG. 2. Free energy at $T^*=3$. The curves are labeled as in Fig. 1.

ability of our theoretical approaches to provide a sensible description of this quantity. However, it must be borne in mind that solid and fluid phases have not been treated on an equal footing. The reference system for the latter, namely, the hard-sphere fluid, is known to be accurately described by the Carnahan-Starling equation of state. In contrast, for the hard-sphere fcc solid phase we have to resort to DFT approaches such as the GELA and MWDA, which will themselves introduce certain inaccuracies. The behavior of MF and MMF approaches will consequently differ in both phases. From the results collected in Table III, one can appreciate that as far as the liquid is concerned, the MMF and MF treatments are comparable, though the MMF seems superior at low temperatures. Nonetheless, these approximations cannot match the RZH results, in particular at low temperatures. This approach, however, is so far unsuitable for phase equilibrium calculations since the optimization procedure and the thermodynamic integration are exceedingly time consuming.

TABLE IV. Coexistence properties of the Heisenberg spin system and the fully aligned system.

Theory	ρ_l^*	ρ_s^*	βp	$\beta\mu$
$T^*=1$				
MC	0.89(2)	1.11(2)	2.01	−2.03
MF				
MMF (GELA)				
MMF (MWDA)				
MC (fully aligned)	0.873	1.113	0.71	−4.38
$T^*=3$				
MC	0.93(2)	1.05(2)	9.20	10.45
MF	0.892	1.023	8.4	8.84
MMF (GELA)	0.883	1.019	8.0	10.8
MMF (MWDA)	0.850	1.039	6.85	9.54

In Figs. 1 and 2 we have plotted the free energy along the two isotherms for which the simulation was performed. Again in the liquid we observe that the MMF theory performs slightly better than the MF approximation. As to the solid, at the higher temperature the combination of the GELA plus the MMF theory reproduces almost exactly the simulation data. When the temperature is lowered, the approximation is not as good, and the results are actually rather poor. Both the GELA with the MMF theory and the MWDA results lie consistently below the simulation data, a situation that is reversed in the liquid phase, and as a consequence the double tangent construction is impossible at $T^*=1$. At this temperature none of the theories predicts an equilibrium between the ferromagnetic liquid and solid phases, but between the paramagnetic gas and the ferromagnetic solid. This is in contrast to the simulation, which clearly indicates that the triple point must lie somewhere below $T^*=1$. The solid-fluid coexistence properties are determined by means of a double tangent construction and for the two isotherms $T^*=1$ and $T^*=3$ are summarized in Table IV. Now the comparison between the various theoretical approaches is more inconclusive. In Fig. 3 we show the complete phase diagram as obtained from the simulation (gas-liquid equilibrium data and the location of the liquid Curie line are taken from Ref. [5]) and in the MMF approach (both using the MWDA and GELA descriptions for the solid). The simulation estimates of Curie line in the solid phase are also shown in the figure. Now the MMF plus GELA seems to be in better agreement with the simulation. Moreover, the combination of the MWDA with the MMF perturbation term with the double minimization strategy proposed by Groh and Dietrich [11] yields in our case a Curie line that considerably deviates from the simulation estimates and departs somewhat from the typical linear behavior. Although the scarcity and uncertainties of the simulation data do not allow for a definite assessment, it seems that the simultaneous optimization of the lattice parameter and the effective field affects the results quite unpredictably. On the other hand, the fact that the GELA predictions for the solid-liquid equilibrium are slightly better is not at all surprising since it simply reflects that this approximation is already somewhat more accurate for the reference system. We note in passing that the MMF Curie line is identical to the MF line in the solid phase, provided the reference system is kept constant for all temperatures, since the temperature at which the transition occurs is so high that the linearization of the exponential in Eq. (17) does not introduce appreciable changes in the results.

Finally, in Fig. 4 we present the complete phase diagram in the mean field approximation, including the Curie lines both in the liquid and in the solid phases. The gas-liquid critical point is clearly underestimated by the MF approach, but aside from this the overall aspect of the phase diagram is quite similar to that obtained using MMF perturbation terms. In both cases the triple point is overestimated by far, i.e., the simulation indicates that the Heisenberg interactions can stabilize the liquid phase to a larger extent than predicted by the theory.

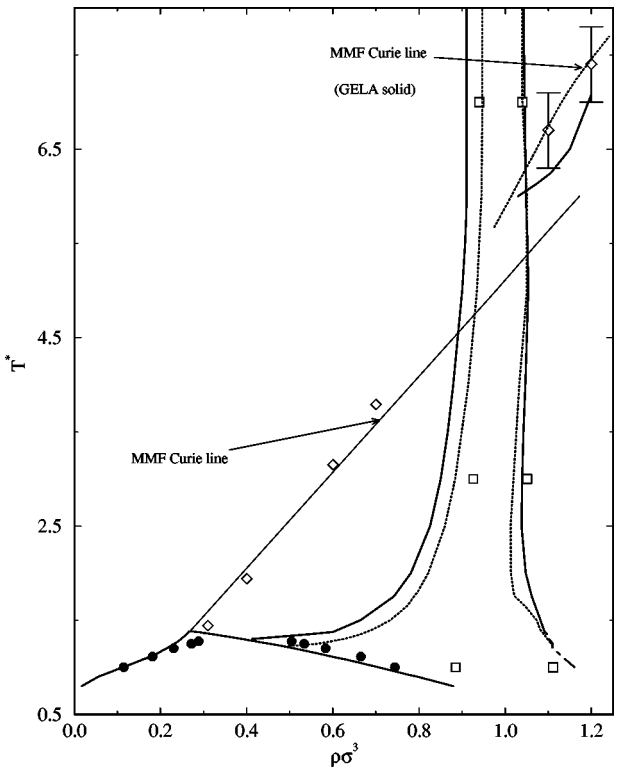

FIG. 3. MMF phase diagram of the Heisenberg spin system. Simulation data are represented by symbols (solid circles are GEMC gas-liquid equilibrium data, squares denote the fluid-solid equilibrium estimates, and diamonds mark the paramagnetic-ferromagnetic transition). Solid lines denote MMF results and the MMF plus the MWDA, and the GELA MMF equilibrium is represented by a dotted line. Fluid-solid data at $T^*=7$ correspond to plain hard spheres.

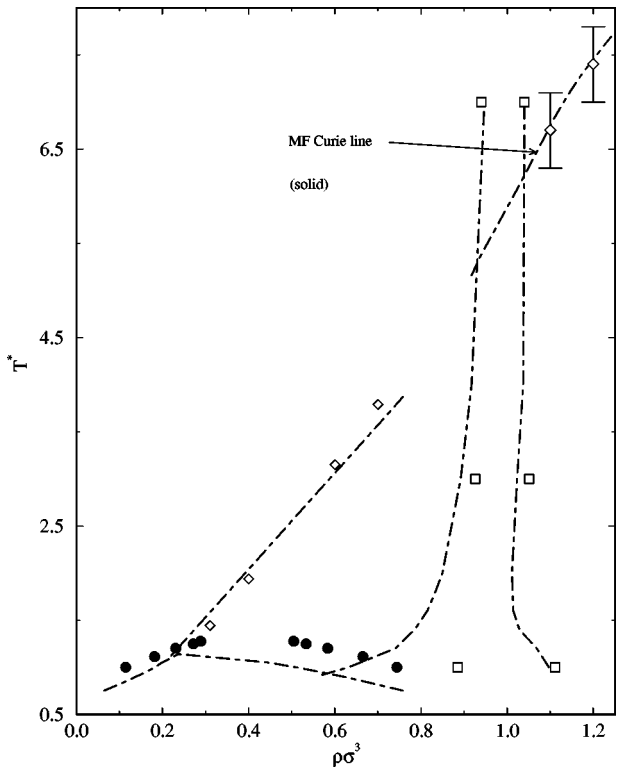

FIG. 4. Mean field phase diagram of the Heisenberg spin system. Simulation data are denoted by symbols as in Fig. 3. The dash-dotted line represents the MF predictions, with the solid described in the GELA.

VI. CONCLUSION

We have presented a complete mapping of the various phases present in the hard-sphere Heisenberg spin system: ferromagnetic and paramagnetic solid, ferromagnetic fluid, and paramagnetic gas. The predictions of various approaches resulting from a combination of DFT and perturbation theory are qualitatively correct, but tend to underestimate the stability of the liquid phase. Most of the discrepancies stem from the poor performance of the theories for the low-temperature ferromagnetic solid, which distorts the shape of the phase diagram. There is much room for improvement here. The liquid phase can be described with extreme accuracy using recently developed integral equation techniques and reasonably well using the DFT approaches just mentioned; however, this will not suffice to attain an accurate mapping of the phase diagram until a better theory for the solid phases becomes available.

ACKNOWLEDGMENTS

E.L. and J.J.W. would like to thank CNRS/CSIC for financial support under their cooperative research agreement. Computing time on the CRAY C-98 was granted by the Institut de Développement et de Ressources en Informatique (IDRIS). The Laboratoire de Physique Théorique et Hautes Energies is Laboratoire Associée au Center National de la Recherche Scientifique (Grant No. URA 063). E.L. and C.F.T. acknowledge support from the Dirección General de Enseñanza Superior (Spain) under Grant No. PB94-0265.

[1] C. Holm and W. Janke, Phys. Rev. B **48**, 936 (1993).
[2] K. Chen, A. M. Ferrenberg, and D. P. Landau, Phys. Rev. B **48**, 3249 (1993).
[3] P. C. Hemmer and D. Imbro, Phys. Rev. E **16**, 380 (1977).
[4] J. M. Tavares, M. M. Telo da Gama, P. I. C. Teixeira, J. J. Weis, and M. J. P. Nijmeijer, Phys. Rev. E **52**, 1915 (1995).
[5] J. J. Weis, M. J. P. Nijmeijer, J. M. Tavares, and M. M. Telo da Gama, Phys. Rev. E **55**, 436 (1997).
[6] M. J. P. Nijmeijer and J. J. Weis, in *Annual Reviews of Computational Physics IV*, edited by D. Stauffer (World Scientific, Singapore, 1996).
[7] E. Lomba, J. J. Weis, N. G. Almarza, F. Bresme, and G. Stell, Phys. Rev. E **49**, 5169 (1994).
[8] M. J. P. Nijmeijer and J. J. Weis, Phys. Rev. Lett. **75**, 2887 (1995); Phys. Rev. E **53**, 591 (1996).
[9] See, e.g., M. P. Allen and D. J. Tildesley, *Computer Simulation of Liquids* (Oxford University Press, London, 1987), and references therein.

[10] B. Groh and S. Dietrich, Phys. Rev. E **50**, 3814 (1994).
[11] B. Groh and S. Dietrich, Phys. Rev. E **54**, 1687 (1996).
[12] S. Klapp and F. Forstmann, Europhys. Lett. **38**, 663 (1997).
[13] A. Oukouiss and M. Baus, Phys. Rev. E **55**, 7242 (1997).
[14] M. A. Osipov, P. I. C. Teixiera, and M. M. Telo da Gama, J. Phys. A **30**, 1953 (1997).
[15] R. Evans, Adv. Phys. **28**, 143 (1979).
[16] R. Evans, in *Fundamentals of Inhomogeneous Fluids*, edited by D. Henderson (Dekker, New York, 1992), p. 85.
[17] M. M. Telo da Gama, Mol. Phys. **52**, 585 (1984).
[18] P. I. C. Teixeira and M. M. Telo da Gama, J. Phys.: Condens. Matter **3**, 111 (1991).
[19] P. Frodl and S. Dietrich, Phys. Rev. A **45**, 7330 (1992).
[20] N. F. Carnahan and K. E. Starling, J. Chem. Phys. **51**, 635 (1969).
[21] J. L. Colot, X. G. Wu, H. Xu, and M. Baus, Phys. Rev. A **38**, 2022 (1988).
[22] J. A. Cuesta, C. F. Tejero, and M. Baus, Phys. Rev. A **39**, 6498 (1989).
[23] *Handbook of Mathematical Functions*, edited by M. Abramowitz and I. A. Stegun (Dover, New York, 1972).
[24] R. Ohnesorge, H. Löwen, and H. Wagner, Europhys. Lett. **22**, 245 (1993).
[25] D. A. Young and B. J. Alder, J. Chem. Phys. **60**, 1254 (1974).
[26] J. F. Lutsko and M. Baus, Phys. Rev. A **41**, 6647 (1990).
[27] C. F. Tejero and J. A. Cuesta, Phys. Rev. E **47**, 490 (1993).
[28] A. R. Denton and N. W. Ashcroft, Phys. Rev. A **39**, 4701 (1989).
[29] C. F. Tejero, M. S. Ripoll, and A. Pérez, Phys. Rev. E **52**, 3632 (1995).
[30] C. F. Tejero, Phys. Rev. E **55**, 3720 (1997).
[31] J. A. C. Veerman and D. Frenkel, Phys. Rev. A **41**, 3237 (1990); P. Bolhuis and D. Frenkel, J. Chem. Phys. **106**, 666 (1997).
[32] K. Binder, Z. Phys. B **43**, 119 (1981).
[33] M. H. J. Hagen and D. Frenkel, J. Chem. Phys. **101**, 4093 (1994).
[34] F. Lado and E. Lomba, Phys. Rev. Lett. **80**, 3535 (1998); F. Lado, E. Lomba, and J. J. Weis, Phys. Rev. E (to be published).
[35] K. R. Hall, J. Chem. Phys. **57**, 2252 (1972).